

Micro- and nanostructured poly[oligo(ethylene glycol)methacrylate] brushes grown from photopatterned halogen initiators by atom transfer radical polymerization

Shah Alang Ahmad^{a)} and Graham J. Leggett^{b)}

Department of Chemistry, University of Sheffield, Sheffield S3 7HF, United Kingdom

Angus Hucknall and Ashutosh Chilkoti^{c)}

Department of Biomedical Engineering, Duke University, P.O. Box 90281, Durham, North Carolina 27708-0281

(Received 29 October 2010; accepted 7 January 2011; published 28 February 2011)

Photolithographic techniques have been used to fabricate polymer brush micro- and nanostructures. On exposure to UV light with a wavelength of 244 nm, halogens were selectively removed from films of chloromethylphenyltrichlorosilane and 3-(2-bromoisobutyramido)propyl-triethoxysilane on silicon dioxide. Patterning was achieved at the micrometer scale, by using a mask in conjunction with the incident laser beam, and at the nanometer scale, by utilizing interferometric lithography (IL). Friction force microscopy images of patterned surfaces exhibited frictional contrast due to removal of the halogen but no topographical contrast. In both cases the halogenated surface was used as an initiator for surface atom-transfer radical polymerization. Patterning of the surface by UV lithography enabled the definition of patterns of initiator from which micro- and nanostructured poly[oligo(ethylene glycol)methacrylate] bottle brushes were grown. Micropatterned brushes formed on both surfaces exhibited excellent resistance to protein adsorption, enabling the formation of protein patterns. Using IL, brush structures were formed that covered macroscopic areas (approximately 0.5 cm²) but exhibited a full width at half maximum height as small as 78 nm, with a period of 225 nm. Spatially selective photolytic removal of halogens that are immobilized on a surface thus appears to be a simple, rapid, and versatile method for the formation of micro- and nanostructured polymer brushes and for the control of protein adsorption. © 2011 American Vacuum Society. [DOI: 10.1116/1.3553579]

I. INTRODUCTION

Polymer brush layers exhibit many attractive characteristics for the control of interfacial interactions. For example, poly(L-lysine)-graft-poly(ethylene glycol) (PEG) films have been reported to yield greatly reduced frictional coefficients during aqueous lubrication under rolling^{1,2} and sliding³ conditions; poly(2-methacryloyloxyethyl phosphoryl choline) brushes have been found to yield high levels of biocompatibility and also to exhibit high levels of lubricity in aqueous media.⁴⁻⁶ Given the potential that polymer brushes offer for the fabrication of sophisticated smart functional films, they are attractive materials for applications in micro- and nanotechnologies.⁷ Some polymer brush systems exhibit exceptionally high levels of resistance to biofouling, a characteristic that is potentially attractive in the context of the fabrication of biochips, where the spatial control of protein adsorption is important. In a biochip, it is necessary to be able to selectively fabricate protein-binding regions in a protein-resistant matrix. A method is thus required to selectively form a protein-resistant brush structure across the surface of the biochip and also to selectively introduce protein-binding regions to enable the formation of sensing elements.

The most widely used protein-resistant materials have been based on PEG⁸ and related materials, including plasma-polymerized tetraglyme [CH₃O(CH₂CH₂O)₄CH₃] (Ref. 9) and self-assembled monolayers of oligo(ethylene glycol) terminated alkanethiolates.¹⁰⁻¹² However, polymer patterning is difficult on small length scales, and while self-assembled monolayers of alkanethiolates,¹³⁻¹⁹ alkylsiloxanes,²⁰⁻²² and alkylphosphonates²³⁻²⁶ have been patterned by a variety of methods, they are not without problems. Alkanethiolate self-assembled monolayers (SAMs) are rarely defect-free and exhibit limited oxidative stability, while siloxane films exhibit low degrees of order. In biological applications, low densities of defects may yield anomalous behavior. For example, proteins may be able to attach to surfaces via very small defects in monolayers. Recently, it has been demonstrated that polymer brushes prepared from oligo(ethylene glycol)methacrylate (OEGMA) exhibit exceptional resistance to protein adsorption.²⁷⁻²⁹ Bottle-brush structures may be synthesized on any surface functionalized with a suitable initiator (usually a bromoisobutyrate group) using atom-transfer radical polymerization (ATRP). For example, the initiator may be attached to gold via a thiol tether and to silicon dioxide by adsorption of a suitable trichlorosilane or by coupling to an aminated siloxane film. Glass is an important

^{a)}Present address: Department of Chemistry, Faculty of Science, Universiti Putra Malaysia, 43400 UPM Serdang, Selangor, Malaysia

^{b)}Electronic mail: graham.leggett@shef.ac.uk

^{c)}Electronic mail: chilkoti@duke.edu

substrate for many applications in biology; the ability to inexpensively render its resistant to protein adsorption is extremely valuable.

To construct functional polymer brush-based micro- and nanostructures, suitable patterning techniques are required. One approach is to form a complete brush film and then to selectively remove polymer material from the surface.³⁰ For example, poly(OEGMA) films may be patterned using selective UV photodegradation by exposure through a mask (for micrometer-scale patterning) or from a near-field optical probe (for nanopatterning).³¹ Alternately, the initiator may first be patterned and the resulting structures may be used as templates from which to grow brushes. For example, micro-contact printing has been used to pattern the attachment of initiators with terminal thiol functionalities on gold surfaces;³² subsequent ATRP yielded brush structures whose dimensions were defined by the pattern of adsorbed initiator molecules.²⁷ Photolithography^{33,34} or micromolding³⁵ may be used to deposit initiator in patterns at the micrometer scale, and brushes subsequently grown, while photobleaching may be used to selectively deactivate photoinitiators for surface-induced polymerization.^{36,37} At smaller length scales, dip-pen nanolithography has been used in an analogous fashion to deposit initiators in patterns from which poly(N-isopropylacrylamide) (NIPAAM) brushes have been grown.^{38,39} Schuh *et al.* fabricated gradients, consisting of a continuously varying density of brushes, by using an interferometer to degrade a photoinitiator-functionalized surface.³⁶

In the present work, we explore a rapid simple approach to brush patterning based on the dehalogenation of a bromo- or chlorofunctionalized surface. Previously it has been reported that benzyl chloride terminated siloxane films may be dehalogenated by exposure to UV light.⁴⁰ However, polymer brush growth from such surfaces has not been demonstrated previously. Here we demonstrate poly(OEGMA) brush growth from patterned benzyl chloride-functionalized siloxane films. We additionally demonstrate that brominated initiator-functionalized monolayers may be dehalogenated in a similar fashion and used as templates for the fabrication of poly(OEGMA) brush layers.

Previously Iwata *et al.* used a short wavelength UV source (185 nm), operating at very high power (15 W for 3.5 h, corresponding to an exposure of approximately 200 kJ) to pattern brominated surfaces from poly[(methacryloyloxy)ethyl phosphorylcholine].⁴¹ Although they showed little x-ray photoelectron spectroscopy (XPS) data and the mechanism of photochemical modification was unclear, it is likely that such aggressive conditions caused complete photolysis of the organic layer in exposed regions. Not only is 185 nm radiation likely to cause C—C bond cleavage, but it may also generate ozone, which would cause oxidative degradation. In the present work we have used XPS to investigate the dose-dependent modification of the halogen initiator film and show that at mild exposures, using longer wavelengths not likely to cause C—C bond cleavage (244 nm), selective dehalogenation may be achieved and

used to form polymer patterns. An additional benefit of the use of chlorobenzyl films is that selective photoconversion of the benzyl chloride to a benzoic acid group is possible, enabling subsequent covalent attachment of proteins.

We also demonstrate the fabrication of nanometer-scale polymer brush patterns by using interferometric lithography (IL) techniques to expose both the chloro- and bromoinitiator films.^{42,43} IL has been widely used for the fabrication of semiconductor structures but has been comparatively little used for patterning molecular materials. It has not previously been used to pattern polymer brush films by selective dehalogenation of initiators. In the present study, a simple bench-top apparatus employing Lloyd's mirror arrangement has been used, in which a coherent laser beam is directed toward a mirror and sample placed at an angular separation of 2θ . Half of the laser beam falls on the mirror, from where it is reflected onto the sample to interfere with the other half of the beam, forming a sinusoidal intensity pattern with period $\lambda/2 \sin \theta$, where λ is the wavelength of the laser beam. IL is an attractive technique for molecular patterning because it offers great simplicity, combined with the capability for exposure of macroscopic (cm^2) regions.

II. EXPERIMENT

A. Preparation of SAMs

Silicon (100) wafers (Goodfellow, Cambridge, UK) were used as substrates. The substrates and glassware were cleaned using piranha solution [30% hydrogen peroxide and concentrated (95%) sulfuric acid in the ratio 3:7]. Caution: Piranha solution has been known to detonate spontaneously upon contact with organic material and therefore great care should be used when handling it. Chlorinated surfaces were prepared following previously published procedure,⁴⁴ by the immersion of silicon wafers in 2.5 mM solution of chloromethylphenyltrichlorosilane (CMPTS) (Fluka) in toluene under a moisture controlled (dry nitrogen) atmosphere. After removal from the solution, the samples were dried with nitrogen and placed in a vacuum oven.

Brominated surfaces [henceforth 3-(2-bromoisobutyramido)propyl-triethoxysilane (BIBAPTES)] were prepared using previously published methodology^{27,28,45,46} by functionalizing films formed by the adsorption of aminopropyl triethoxysilane using bromoisobutyryl bromide. All reagents were purchased from Sigma-Aldrich. A two-step process was used. Substrates were first immersed in a 10% solution of 3-aminopropyltriethoxysilane in ethanol for 30 min. They were then rinsed with ethanol and dried at 120 °C. In the second step, the resulting films were immersed in a solution of bromoisobutyryl bromide (1%) and triethylamine (1%) in dichloromethane for 30 min, followed by rinsing with ethanol and dichloromethane and drying under N_2 .

B. UV modification

UV exposure was carried out using a frequency-doubled argon ion laser (Coherent Innova FreD300C) with a wave-

length of 244 nm. The beam was expanded using a beam expander so that the area exposed was 0.8 cm². Micropatterning was accomplished by exposing the samples through a Cu electron microscope grid (Agar, Cambridge, UK). IL was carried out using a two-beam interference system (Lloyd's mirror).⁴²

C. Preparation of poly(OEGMA) brushes

Following exposure to UV light, polymer brushes were prepared by immersing the samples for 12 h in a degassed 20% water in methanol (*v/v*) solution of 5 mg mL⁻¹ Cu(I)Br, 12 mg mL⁻¹ bipyridine, and 300 mg mL⁻¹ oligo(ethylene glycol) methacrylate under argon. After removal from solution, the samples were then rinsed with de-ionized water and dried under a stream of N₂.

D. Surface activation

Carboxylic acid terminated surfaces generated by UV irradiation were activated using *N*-(3-dimethylaminopropyl)-*N'*-ethylcarbodiimide (EDC) and *N*-hydroxysuccinimide (NHS). The samples were immersed in a solution of 100 mM EDC and 100 mM NHS in dimethylformamide (DMF) for 20 min as described in the literature.⁴⁷ The chemicals were obtained from Sigma-Aldrich. DMF solvent was supplied by the Grubbs dry solvent system.

E. Protein immobilization

The activated surfaces were incubated in a solution of NeutrAvidin nanoparticles in phosphate-buffered saline (PBS) solution at concentration of approximately 10 μg mL⁻¹ in the dark for 2 h and then rinsed with PBS buffer solution followed by de-ionized water and dried gently under nitrogen.

F. Surface characterization

Sessile drop contact angle measurements were made using a Rame-Hart model 100-00 contact angle goniometer. Contact-mode topographical and friction force measurements were made using a Digital Instruments Ltd. Multimode Nanoscope IIIA atomic force microscope (Digital Instruments, Cambridge, UK). Silicon nitride nanoprobes (Digital Instruments, Cambridge, UK) with nominal force constants of 0.06 and 0.12 N m⁻¹ were used. XPS was carried out using a Kratos axis ultra-delay line detector (DLD) x-ray photoelectron spectrometer (Kratos Analytical, Manchester, UK) equipped with a monochromatic Al K α x-ray source in an ultrahigh-vacuum environment. The high-resolution spectra were acquired at a pass energy of 20 eV. CASAXPS software (Casa Software Ltd., <http://www.casaxps.com>) was used to analyze the data. Fluorescence microscopy images were acquired after immersion of samples in NeutrAvidin solution, using a LSM 510 laser scanning confocal microscope (Carl Zeiss, Welwyn Garden City, UK) and a 488 nm Ar ion laser. A 40 \times magnification oil immersion lens was used for imaging the samples, which were mounted in an antifade reagent (glycerol-PBS solution, AF1) (Citifluor Ltd.,



FIG. 1. (Color online) AFM images of initiator-functionalized surfaces: (a) 5 \times 5 μm^2 image of a film formed from CMPTS; (b) 10 \times 10 μm^2 image of a film formed from 3-(2-bromoisobutyramido)propyl-triethoxysilane. Vertical contrast range: 0–10 nm in both images.

London, UK). The captured images were analyzed using Zeiss LSM image browser software.

III. RESULTS AND DISCUSSION

A. Characterization of initiator films

Figure 1 shows atomic force microscopy (AFM) topographical images of films formed from CMPTS and BIBAPTES. The root mean square roughnesses of the two films, measured across the entire image area, were 0.6 and 0.7 nm, respectively. The smooth morphology of these samples is consistent with the formation of high quality films. A contact angle of 79 $^\circ$ was measured for CMPTS, while a value of 67 $^\circ$ was measured for BIBAPTES.

Figure 2 shows XPS C 1s spectra of the films. For CMPTS, the spectrum was fitted using two components, corresponding to the C—C and C—H hydrocarbon peaks at 285.0 eV and the C—Cl shoulder at 287.2 eV. The relative areas of the two components (83% and 17%, respectively) were consistent with the expected composition of the film. For BIBAPTES, curve fitting of the C 1s core level spectrum

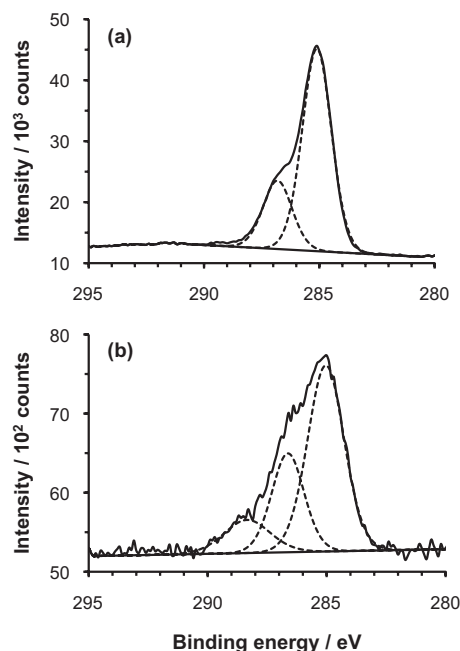


FIG. 2. C 1s XPS spectra for (a) CMPTS and (b) BIBAPTES.

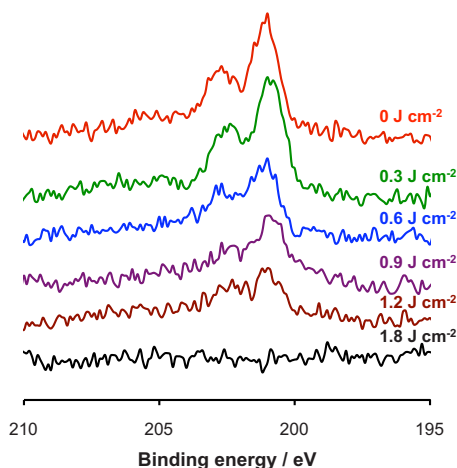


FIG. 3. (Color online) Changes in the XPS Cl $2p$ spectrum of CMPTS following exposure to UV light.

yielded three components at binding energies of 285.0, 286.3, and 288.3 eV, attributable to the C—C, C—Br/C—NCO, and O=C—N, respectively. The predicted ratio of C—C:C—Br/NCO:O=C—N is 4:2:1 and this was consistent with the ratios obtained from the C $1s$ spectrum. Peaks were also observed, as expected, for N and Br (not shown).

B. UV modification

The UV modification of CMPTS films in air has previously been reported by Sun *et al.*⁴⁰ In agreement with their work, it was found that following a UV exposure of approximately 3 J cm^{-2} , the water contact angle declined to 20° and the C $1s$ region of the XPS spectrum exhibited new peaks due to aldehyde and carboxylate functionalities and a loss of the C—Cl component. However, Sun *et al.* did not study the change in the Cl $2p$ peak accompanying these changes. Therefore, because of the importance of Cl as an initiator in the present study, Cl $2p$ spectra were acquired as a function of UV exposure (Fig. 3).

The Cl $2p$ core level spectrum of the unmodified material consisted of Cl $2p_{3/2}$ and Cl $2p_{1/2}$ components at binding energies of approximately 199.9 and 201.5 eV, respectively, which are characteristic of covalently bound chlorine species. The relative intensity of the components of the doublet formed by the spin-orbit coupling is defined by the expression $(2j+1)$. Thus, the relative intensities of $\frac{1}{2}$ and $\frac{3}{2}$ peaks were 1:2. The intensity of the Cl $2p$ peak decreased following UV irradiation because of Cl—C bond cleavage following exposure to UV light. It declined to an undetectable level after an exposure of 1.8 J cm^{-2} (6 min). The carboxylate component became dominant in the C $1s$ spectrum at a higher exposure of approximately 3 J cm^{-2} .

The change in contact angle following irradiation of BIBAPTES films was modest, reducing from 67° to approximately 56° after an exposure of 1.5 J cm^{-2} (5 min). However, significant changes were observed in the XPS spectrum. In the C $1s$ region, a decrease was observed in the

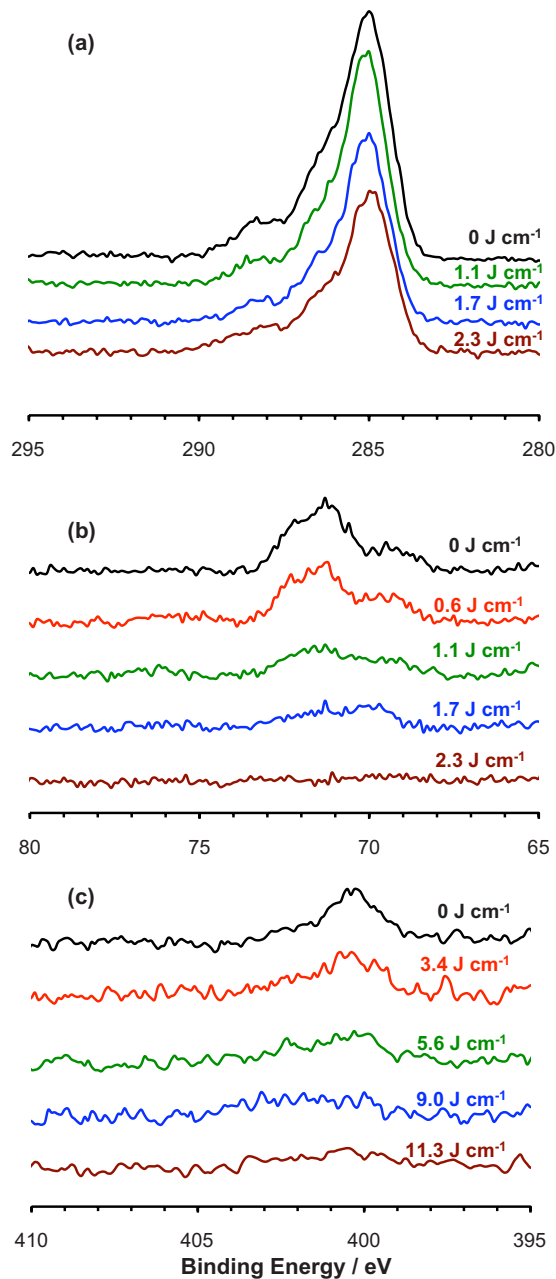


FIG. 4. (Color online) Changes in (a) the C $1s$ region, (b) the Br $3d$ region, and (c) the N $1s$ region of BIBAPTES films following UV exposure.

intensity of the components due to C—Br and C—N at 286.5 eV with increasing UV exposure, suggesting photolysis had occurred. The intensity of the Br $3d$ band diminished as the UV irradiation time increased, indicating removal of the halogen atom. After a 2 min exposure at a power of 15 mW, corresponding to a dose of 2.3 J cm^{-2} , the Br $3d$ signal had declined to negligible intensity [Fig. 4(b)]. In the N $1s$ region, there was no change in the spectrum for exposures up to 3.4 J cm^{-2} (3 min). However, at larger exposures, the band slowly reduced in intensity with increasing UV exposure, and it eventually disappeared after 10 min of UV irradiation (2.3 J cm^{-2}), likely resulting from ablation of the adsorbate from the surface.

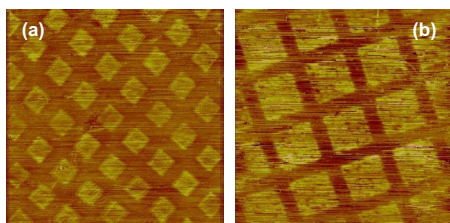


FIG. 5. (Color online) Friction force microscopy images of patterned samples. (a) Micropatterned CMPTS, $100 \times 100 \mu\text{m}^2$, and z -range of 0–7 V. (b) Micropatterned BIBAPTES, $100 \times 100 \mu\text{m}^2$, and z -range of 0–1 V.

Micrometer-scale patterning was carried out by exposing the CMTS and BIBAPTES functionalized glass through a mask (an electron microscope grid). Friction force microscopy (FFM) was used to image the resulting patterns. Figure 5(a) shows a CMPTS sample following exposure through a 1500 mesh grid ($1500 \text{ lines in.}^{-1}$) to 1.8 J cm^{-2} (6 min), corresponding to full removal of the Cl. There is clear contrast between the masked regions (bars) and the exposed areas (squares), with the exposed areas exhibiting the brightest contrast, suggesting a larger coefficient of friction in these areas. This is explained by the difference in surface free energy between the two regions: the exposed areas are more polar and hence the AFM probe adheres more strongly to these regions, resulting in a higher rate of energy dissipation and hence a larger coefficient of friction. Figure 5(b) shows a BIBAPTES sample that was similarly patterned using a 1000 mesh grid at a dose of 2.3 J cm^{-2} , conditions that cause complete removal of the Br. The contrast in this image was similarly brighter in the exposed areas than in the masked ones, but the difference in contrast between UV-irradiated and unexposed areas was much smaller than was the case for the CMPTS modified surface, as the contrast range in Fig. 5(b) is one seventh that in Fig. 5(a), consistent with the much smaller change in contact angle following UV exposure.

C. Growth of poly-OEGMA brushes

Surface ATRP was used to grow polymer brushes from the patterned initiator surfaces. Prior to brush growth, the patterned surfaces did not show any height contrast between the irradiated and nonirradiated regions. After polymerization, AFM analysis revealed a pattern of varying contrast, reflecting spatially organized growth of polymer brushes on the patterned chlorinated and brominated surfaces as illustrated in Figs. 6(a) and 6(b), respectively. Regions that had been masked during exposure (the bars) exhibited brighter height contrast than regions that had been exposed to UV light (squares), indicating that brush growth occurred from the regions where the halogens remained intact and not from the exposed areas where the halogens had been removed. Clear boundaries were observed between the grafted poly[oligo(ethylene glycol)methacrylate] (POEGMA) brushes (bars) and the exposed areas (squares). The cross-sectional profiles reveal that the average height differences between the grafted brushes and the regions from which the chlorine and bromine initiators have been removed are 4.4 ± 2.4 and

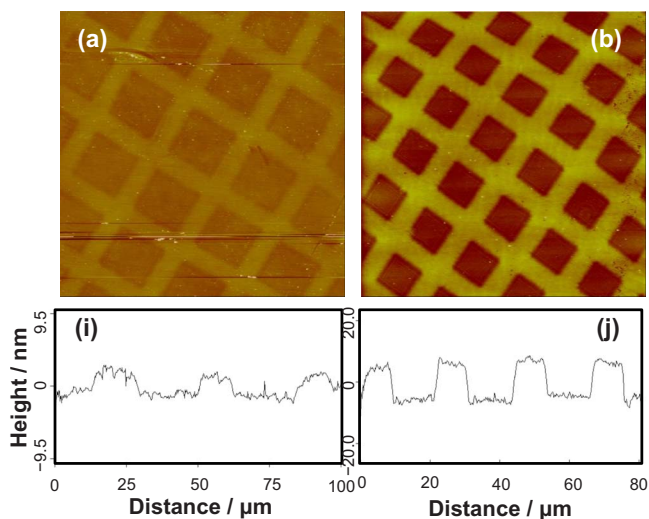


FIG. 6. (Color online) AFM height images in contact mode of micropatterned POEGMA brushes polymerized on patterns of (a) CMPTS and (b) BIBAPTES. A representative cross section is shown for each sample. Image sizes: (a) $100 \times 100 \mu\text{m}^2$; (b) $80 \times 80 \mu\text{m}^2$.

$14.1 \pm 0.7 \text{ nm}$, respectively, indicating that the degree of polymerization is greater, for a given reaction time, for the brominated surfaces than for the chlorinated ones.

D. Immobilization of proteins on patterned surfaces

To test the resistance of the POEGMA brush-patterned surfaces toward proteins, micropatterned samples, onto which POEGMA brushes had first been grown, were immersed in solutions of NeutrAvidin particles (dye-labeled avidin-coated latex particles). Because the exposure used for the CMPTS system was sufficient to convert the adsorbate terminal groups to carboxylic acids,⁴⁰ these samples were first activated using a water-soluble carbodiimide and *N*-hydroxysuccinimide to create a surface-bound active ester group. The BIBAPTES samples were not activated because the precise nature of the terminal group chemistry following UV exposure was not known. Figure 7 shows fluorescence micrographs of the resulting samples, together with cross sections indicating the fluorescence intensity across the patterns. The contrast difference between the exposed areas (squares) and the masked areas (bars) is clear, indicating that the brushes grown on the masked areas resist protein adsorption effectively, while the brush-free exposed areas bind proteins effectively. The similarity in the fluorescence signal intensity difference between the masked and exposed areas for the two samples (approximately 100 units) suggests little difference in the amount of protein bound to the active ester-derivatized COOH surface and the degraded R—Br of unknown chemistry.

E. Nanofabrication

We next tested the possibility of using IL to photolytically pattern ATRP initiators with nanoscale resolution. IL is an attractive technique for molecular patterning because it is simple and can potentially enable the growth of nanostruc-

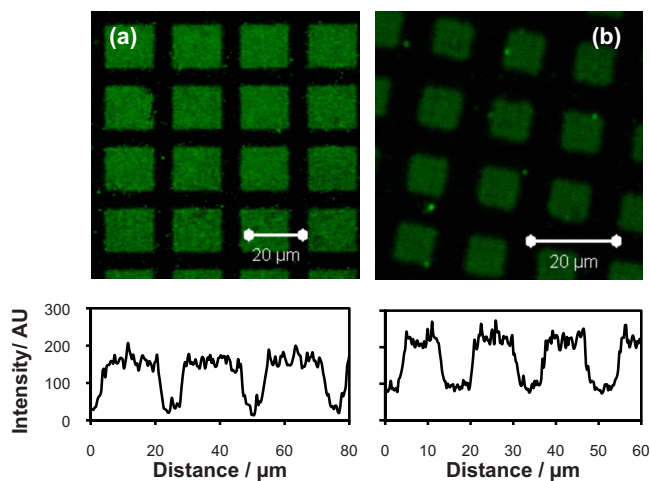


FIG. 7. (Color online) Fluorescence micrographs of patterned POEGMA on glass following immersion in a solution of NeutrAvidin particles. (a) CMPTS, following UV exposure, POEGMA brush growth, and NHS/carbodiimide activation; (b) BIBAPTES following UV exposure and POEGMA brush growth only. NB. Differences in feature sizes result from the use of different masks, not process differences.

tured polymer brushes from patterned ATRP initiators over macroscopic (cm^2) region. A simple bench-top apparatus employing Lloyd's mirror arrangement using a two-beam interference system⁴² was used to fabricate patterns of immobilized CMPTS and BIBAPTES as follows: a coherent laser beam was directed toward a mirror and sample placed at an angular separation of 2θ . Half of the laser beam falls on the mirror, from where it is reflected onto the sample to interfere with the other half of the beam, forming a sinusoidal intensity pattern with period $\lambda/2 \sin \theta$, where λ is the wavelength of the laser beam. We sought to examine whether this sinusoidal pattern of optical intensity could be used to photolytically pattern the immobilized ATRP initiators with nanoscale spatial resolution.

Figures 8(a) and 8(c) show FFM images of a CMPTS-functionalized glass substrate following exposure using the interferometer. The dose was 3 J cm^{-2} . Bands of alternating high and low contrasts are observed. The bright bands, with widths of $150 \pm 2.8 \text{ nm}$, correspond to regions of extensive modification, while the dark bands, $75 \pm 1.5 \text{ nm}$ wide, correspond to regions of low modification. Topographical images (acquired simultaneously with the FFM images) showed no height contrast, indicating no ablation of material had occurred (via Si—C bond cleavage). For BIBAPTES [Figs. 8(b) and 8(d)], FFM images also exhibited patterns of alternating bright and dark contrasts, indicating that the patterns were also well defined with the bright and dark bands having widths of 102.3 ± 3.3 and $136.0 \pm 5.9 \text{ nm}$, respectively.

Polymerization of OEGMA by ATRP was then carried out on the patterned surfaces to test the feasibility of growing nanoscale polymer brush structures from the photopatterned substrates. Figures 8(e)–8(h) show contact mode AFM height images of the resulting structures. In regions where the initiator was exposed to UV light and thus dehalogenated, the brushes did not grow, yielding dark contrast, while in regions

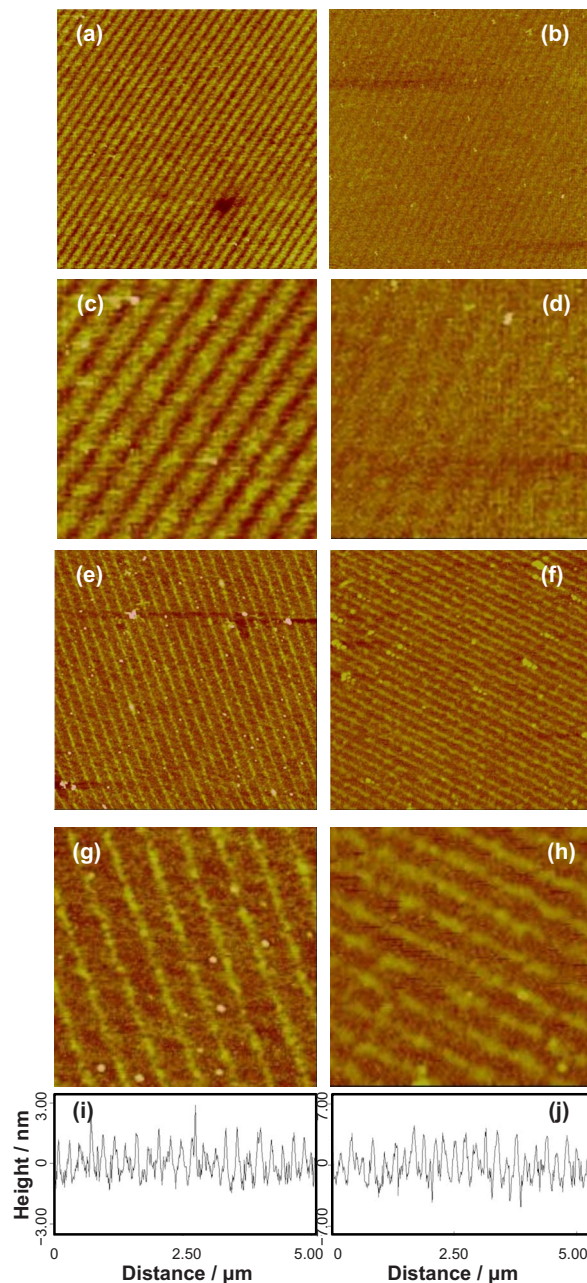


FIG. 8. (Color online) (a) FFM image of nanopatterned CMPTS, $5.7 \times 5.7 \mu\text{m}^2$, and z -range of 0–7 V. (b) FFM image nanopatterned BIBAPTES, $5.7 \times 5.7 \mu\text{m}^2$, and z -range of 0–1 V. (c) and (d) FFM images of $1.9 \times 1.9 \mu\text{m}^2$ regions shown in (a) and (b), respectively, at higher magnification. (e) Contact-mode topographical AFM image of nanopatterned POEGMA brushes formed on IL-patterned films of CMPTS (image size $5 \times 5 \mu\text{m}^2$ and z -contrast range of 0–10 nm). (f) Contact-mode topographical AFM image of nanopatterned POEGMA brushes formed on IL-patterned films of BIBAPTES (image size $5 \times 5 \mu\text{m}^2$ and z -contrast range of 0–15 nm). (g) and (h) Topographical images of $1.9 \times 1.9 \mu\text{m}^2$ regions shown in (e) and (f), respectively, at higher magnification. (i) and (j) Line sections through (e) and (f), respectively.

where the initiator remained intact, brush growth occurred. By using a comparatively high exposure, it was possible to thin the bands of intact initiator thus enabling the growth of very narrow brush structures that were extended over macroscopic areas (approximately $5 \times 5 \text{ mm}^2$). The topographi-

cal images in Figs. 8(e) and 8(f) show, respectively, POEGMA structures grown on chlorinated and brominated surfaces with linewidths (full width at half maximum) of 78 ± 5.6 and 105 ± 9.4 nm, respectively, and heights of 2.1 ± 0.5 and 5.44 ± 0.7 nm, respectively. These are mean values, determined from analysis of a large number of cross sections. Brushes grown from the nanolines were found to be thinner than those grown from the micropatterns under similar conditions. Kaholek *et al.* also noted that their nanopatterned brushes exhibited smaller heights than bulk films patterned under identical conditions.³⁹ They attributed this to the lower density of brushes in the nanostructures. Our data suggest similar behavior: close packing of polymer chains is required to achieve a dense upright brush, but for small structures, as the line width starts to approach the radius of gyration of the polymer, this is much harder to achieve. The linewidth was greater for the structures grown from the brominated surfaces because the degree of polymerization and hence the polymer chain length were greater. Consequently, collapse of the nanostructured brushes yields a broader structure than is the case for the shorter brushes grown from the chlorinated surfaces.

Schuh *et al.* previously used IL to pattern photoinitiator molecules in order to fabricate gradient structures.³⁶ They exploited the smooth continuous gradient of exposure available in an interferometer to yield a well-defined gradient of brush grafting density. They utilized a photoinitiator to polymerize acrylamide, while we have employed a halogen initiator for ATRP. However, in both cases, IL has yielded well-defined structures in which surface polymerization is controlled at high precision over nanometer length scales. In contrast to electron beam lithography, which requires expensive infrastructure and scanning probe techniques, for which patterning over macroscopic areas remains (with few exceptions) challenging, IL offers the possibility for rapid fabrication of molecular and macromolecular nanostructures over macroscopic areas using simple readily available apparatus.

IV. SUMMARY AND CONCLUSIONS

Exposure of CMPTS and BIBAPTES films to UV light leads to dehalogenation in a rapid process. We have shown that the immobilized CMPTS and BIBAPTES can be photopatterned through the use of either an optical mask or an interferometer. Friction force microscopy measurements of patterned ATRP initiators revealed friction contrast, resulting from the change in surface chemistry due to dehalogenation, but no topographical contrast, indicating that the removal of the halogen atom is quite selective. Polymer brushes were grown from unmodified regions of the resulting patterns, but not from the dehalogenated areas. Micrometer-scale brush structures fabricated in a mask-based lithographic process exhibited excellent resistance to the adsorption of protein-coated NeutrAvidin particles. At the same time, brushes grown on brominated surfaces were found to be approximately three times thicker than brushes grown from halogenated surfaces. Nanometer-scale brush structures were also fabricated over macroscopic areas using interferometric li-

thography. The process was rapid and simple and yielded full widths at half maximum height of 78 and 105 nm for chlorinated and brominated surfaces, respectively. In conclusion, UV photopatterning of halogenated ATRP initiators appears to provide a simple rapid route to the fabrication of brush structures with sizes ranging from micrometers to nanometers.

ACKNOWLEDGMENTS

One of the authors (S.A.A.) thanks the Malaysian Government for a research scholarship. Two of the authors (G.J.L. and S.A.A.) thank RCUK (Grant No. EP/C523857/1), EPSRC, and RSC Analytical Chemistry Trust Fund for support.

- ¹S. Lee, M. Müller, M. Ratoi-Salagean, J. Vörös, S. Pasche, S. M. D. Paul, H. A. Spikes, M. Textor, and N. D. Spencer, *Tribol. Lett.* **15**, 231 (2003).
- ²M. Müller, S. Lee, H. A. Spikes, and N. D. Spencer, *Tribol. Lett.* **15**, 395 (2003).
- ³T. Drobek and N. D. Spencer, *Langmuir* **24**, 1484 (2008).
- ⁴M. Chen, W. H. Briscoe, S. P. Armes, and J. Klein, *Science* **323**, 1698 (2009).
- ⁵K. Kitano, Y. Inoue, R. Matsuno, M. Takai, and K. Ishihara, *Colloids Surf., B* **74**, 350 (2009).
- ⁶A. J. Morse, S. Edmondson, D. Dupina, S. P. Armes, Z. Zhang, G. J. Leggett, R. L. Thompson, and A. L. Lewis, *Soft Matter* **6**, 1571 (2010).
- ⁷F. Zhou and W. T. S. Huck, *Phys. Chem. Chem. Phys.* **8**, 3815 (2006).
- ⁸J. M. Harris, *Poly(Ethylene Glycol) Chemistry: Biochemical and Biomedical Applications* (Plenum, New York, 1992).
- ⁹G. P. López, B. D. Ratner, C. D. Tidwell, C. L. Haycox, R. J. Rapoza, and T. A. Horbett, *J. Biomed. Mater. Res.* **26**, 415 (1992).
- ¹⁰C. Pale-Grosdemange, E. S. Simon, K. L. Prime, and G. M. Whitesides, *J. Am. Chem. Soc.* **113**, 12 (1991).
- ¹¹E. Ostuni, R. G. Chapman, E. R. Holmlin, S. Takayama, and G. M. Whitesides, *Langmuir* **17**, 5605 (2001).
- ¹²P. Harder, M. Grunze, R. Dahint, G. M. Whitesides, and P. E. Laibinis, *J. Phys. Chem. B* **102**, 426 (1998).
- ¹³R. D. Piner, J. Zhu, F. Xu, S. Hong, and C. A. Mirkin, *Science* **283**, 661 (1999).
- ¹⁴S. Hong, J. Zhu, and C. A. Mirkin, *Science* **286**, 523 (1999).
- ¹⁵K.-B. Lee, S.-J. Park, C. A. Mirkin, J. C. Smith, and M. Mrksich, *Science* **295**, 1702 (2002).
- ¹⁶K. Salaita, Y. Wang, J. Fragala, R. A. Vega, C. Liu, and C. A. Mirkin, *Angew. Chem., Int. Ed.* **45**, 7220 (2006).
- ¹⁷S. Sun, K. S. L. Chong, and G. J. Leggett, *J. Am. Chem. Soc.* **124**, 2414 (2002).
- ¹⁸S. Sun and G. J. Leggett, *Nano Lett.* **4**, 1381 (2004).
- ¹⁹M. Montague, R. E. Ducker, K. S. L. Chong, R. J. Manning, F. J. M. Rutton, M. C. Davies, and G. J. Leggett, *Langmuir* **23**, 7328 (2007).
- ²⁰R. Maoz, E. Frydman, S. R. Cohen, and J. Sagiv, *Adv. Mater.* **12**, 725 (2000).
- ²¹R. Maoz, E. Frydman, S. R. Cohen, and J. Sagiv, *Adv. Mater.* **12**, 424 (2000).
- ²²S. Hoepfener, R. Maoz, and J. Sagiv, *Nano Lett.* **3**, 761 (2003).
- ²³R. S. Dibbell, G. S. Soja, R. M. Hoth, and D. F. Watson, *Langmuir* **23**, 3432 (2007).
- ²⁴G. R. Soja, J. R. Mann, and D. F. Watson, *Langmuir* **24**, 5249 (2008).
- ²⁵G. R. Soja and D. F. Watson, *Langmuir* **25**, 5398 (2009).
- ²⁶G. Tizazu, A. Adawi, G. J. Leggett, and D. G. Lidzey, *Langmuir* **25**, 10746 (2009).
- ²⁷H. Ma, D. Li, X. Sheng, B. Zhao, and A. Chilkoti, *Langmuir* **22**, 3751 (2006).
- ²⁸H. Ma, M. Wells, T. P. Beebe, Jr., and A. Chilkoti, *Adv. Funct. Mater.* **16**, 640 (2006).
- ²⁹A. Hucknall, S. Rangarajan, and A. Chilkoti, *Adv. Mater.* **21**, 2441 (2009).
- ³⁰M. Husemann, M. Morrison, D. Benoit, J. Frommer, C. M. Mate, W. D. Hinsberg, J. L. Hedrick, and C. J. Hawker, *J. Am. Chem. Soc.* **122**, 1844

- (2000).
- ³¹S. Alang Ahmad, A. Hucknall, A. Chilkoti, and G. J. Leggett, *Langmuir* **26**, 9937 (2010).
- ³²F. Zhou, Z. Zheng, B. Yu, W. Liu, and W. T. S. Huck, *J. Am. Chem. Soc.* **128**, 16253 (2006).
- ³³Y. Zou, P.-Y. J. Yeh, N. A. A. Rossi, D. E. Brooks, and J. N. Kizakke-dathu, *Biomacromolecules* **11**, 284 (2010).
- ³⁴M. Mathieu, A. Friebe, S. Franzka, M. Ulbricht, and N. Hartmann, *Langmuir* **25**, 12393 (2009).
- ³⁵Y. Liu, V. Klep, and I. Luginov, *J. Am. Chem. Soc.* **128**, 8106 (2006).
- ³⁶C. Schuh, S. Santer, O. Prucker, and J. Ruhe, *Adv. Mater.* **21**, 4706 (2009).
- ³⁷X. Jia, X. Jiang, R. Liu, and J. Yin, *ACS Appl. Mater. Interfaces* **2**, 1200 (2010).
- ³⁸M. Kaholek, W.-K. Lee, B. LaMattina, K. C. Caster, and S. Zauscher, *Nano Lett.* **4**, 373 (2004).
- ³⁹M. Kaholek, W.-K. Lee, J. Feng, B. LaMattina, D. J. Dyer, and S. Zauscher, *Chem. Mater.* **18**, 3660 (2006).
- ⁴⁰S. Sun, M. Montague, K. Critchley, M.-S. Chen, W. J. Dressick, S. D. Evans, and G. J. Leggett, *Nano Lett.* **6**, 29 (2006).
- ⁴¹R. Iwata, P. Suk-In, V. P. Hoven, A. Takahara, K. Akiyoshi, and Y. Iwasaki, *Biomacromolecules* **5**, 2308 (2004).
- ⁴²S. R. J. Brueck, *Proc. IEEE* **93**, 1704 (2005).
- ⁴³C. Lu and R. H. Lipson, *Laser Photonics Rev.* **1**, 568 (2009).
- ⁴⁴S. Alang Ahmad, L. S. Wong, E. Ul-Haq, J. K. Hobbs, G. J. Leggett, and J. Micklefield, *J. Am. Chem. Soc.* **131**, 1513 (2009).
- ⁴⁵H. Ma, M. Textor, R. L. Clark, and A. Chilkoti, *BioInterphases* **1**, 35 (2006).
- ⁴⁶A. Hucknall, A. J. Simnick, R. T. Hill, A. Chilkoti, A. Garcia, M. S. Johannes, R. L. Clark, S. Zauscher, and B. D. Ratner, *BioInterphases* **4**, FA50 (2009).
- ⁴⁷R. E. Ducker and G. J. Leggett, *J. Am. Chem. Soc.* **128**, 392 (2006).